Article

Not peer-reviewed version

Novel Bone Void Filling Cement Compositions based on Shell Nacre and Siloxane Methacrylate Resin: Development and Characterization

Bridget Jeyatha W and Lizymol P.P. *

Posted Date: 6 May 2023

doi: 10.20944/preprints202305.0422.v1

Keywords: shell nacre; ormocer; bone void filling cement; bone defects

Article

Novel Bone Void Filling Cement Compositions Based on Shell Nacre and Siloxane Methacrylate Resin: Development and Characterization

Bridget Jeyatha W. and Lizymol P.P. *

Division of Dental Products, Department of Biomaterial Science and Technology, Biomedical Technology Wing, Sree Chitra Tirunal Institute for Medical Sciences and Technology, Kerala, India

* Correspondence: lizymol@sctimst.ac.in

Abstract: Shell nacre from *Pinctada* species has been extensively researched for managing bone defects. However, there is a gap in the research on using shell nacre as cement with improved physicochemical properties. To address this, the current study aimed to develop a chemical curable composite shell nacre cement (SNC) using shell nacre powder and an organically modified ceramic resin shell nacre containing ladder-structured siloxane methacrylate (SNLSM). Different amounts of shell nacre (24, 48, and 72 weight(wt)%) were added to the SNLSM resin matrix and the effect on the physicochemical properties of the cement was studied. The composite shell nacre cement SNC 72 containing 72 wt% shell nacre exhibited significantly higher mechanical properties (compressive strength >100 MPa, flexural strength > 35 MPa) and low linear polymerization shrinkage (0.4%) than other compositions. SNC 72 was radiopaque and the exotherm generated during the curing of the cement was minimal. Direct contact of cured SNC 72 with L929 cells revealed the non-cytotoxic nature of the cement. Overall, the results of the study proved that the composite SNC 72 would be a promising candidate for bone defect management.

Keywords: shell nacre; ormocer; bone void filling cement; bone defects

1. Introduction

The management of bone defects depends on the size, shape, and location of the defect as well as on the health conditions and age of the patients. The main aim of the management of metaphyseal defects is to provide mechanical support for the joint surface and to restore bone stock**.** Irregular bone defects that are less than 5mm or between 5-10mm in size are treated with either bone cement or bone cement with screw augmentation [1–3]. Polymethyl methacrylate **(**PMMA) cement is the most studied and clinically used material for the management of fragility fractures[4], vertebral compression fractures [5] revision arthroplasty defects, and bone voids after infection [6]/ tumor resections [7], *etc*. It is a multifunctional material that acts as a stabilizer for stabilizing the vertebral fractures during vertebroplasty, kyphoplasty, and vertebral stenting procedures, filler for filling bone defects; spacer for the treatment of segmental defects in the Masquelet technique; and carrier of drugs for the treatment of bone tumor and infections. Apart from its inert application in arthroplasty, it is used solely for its mechanical properties, regardless of the potential toxicity of the monomer or the exotherm generated during polymerization[8–10]. In an attempt to reduce polymerization shrinkage and exotherm generation, several organic matrices have been studied, such as poly(ethylene) glycol dimethacrylate [9], terpolymer of bisGMA, bisphenol-A-ethoxy dimethacrylate (bis-EMA) and TEGDMA [10], polyacrylic acid and styrene [13], bisphenol-A-glycidyl methacrylate (Bis GMA), triethylene glycol dimethacrylate (TEGDMA)[5], and urethane dimethacrylate (UDMA)[8] *etc.* With the concept of bioactivity, many researchers modified the cement formula with silanated glass[11], apatite wollastonite glass ceramic (AW-GC) [12], nano-sized titania particles [13], hydroxyapatite [14], strontium substituted hydroxyapatite [15], hydroxyapatite along with BMP-2 [16], synthetic combeite glass-ceramic particles, barium boro aluminosilicate glass and silica particles[17],

borosilicate glass [18] and graphene oxide [19] *etc.* Osteoconductive cement such as calcium phosphate, calcium sulfate, tricalcium phosphate, calcium silicate and magnesium phosphate cement have also been investigated. However, brittleness, low mechanical properties, and faster resorption of these cements may not provide the long-term mechanical support required[20–27]. So, the poor biological performance of PMMA-based cements and the lower mechanical performance of self-setting cements emphasize the critical need for an alternative cement that can offer both better biological and mechanical properties.

Shell nacre/mother of pearl is the inner nacreous layer of pearl oyster shell composed of calcium carbonate crystals arranged in aragonite form with an organic layer inter-tiled between them in a brick-and-mortar fashion. The *in vitro* osteogenesis of shell nacre without any inducer is first revealed by Lopez *et al*., 1989[28] followed by Camprasse *et al.* who developed an artificial dental root made of calcium carbonate(Bioracine)[29]. A comparison study proved that shell nacre induced new bone formation whereas PMMA caused necrosis and reduced bone mineralization [30]. Besides osteogenesis, radiopacity, osseo-integration [28], high fracture toughness and strength, biodegradability[31], anti-osteoporotic activity[32] and angiogenesis property [33] proved shell nacre as a suitable biomaterial for hard tissue applications [34]. It is either studied as a bone substitute or as a powder mixed with blood or the water soluble matrix[34,35]. There is no processing method to get shell nacre powder with both organic and inorganic part.

Organically modified ceramic resin (ORMOCER) is a three-dimensional multifunctional inorganic-organic hybrid resin [36] used in the field of dental cements for non-cytotoxic nature, low polymerization shrinkage and mechanical properties[37–40]. It is easily synthesized by modified sol gel method using methacrylate substituted alkoxysilanes through the process of hydrolysis and condensation to form the inorganic siloxane network whereas the methacrylate moieties remain intact [41]. Cage/random/ladder structured siloxane network is formed depending upon the catalyst used [42,43]. Later the methacrylate groups undergoes photo/chemical curing to form the organic network [44]. In our previous study, it was reported that photocured cement of ladder structured siloxane methacrylate (LSM) resin exhibited low shrinkage properties [45]. Hence, in this study shell nacre containing SN-LSM resin was synthesized and used to set the shell nacre powder as a bone void filling cement.

The main objective of the study was to develop an *in situ* curing bone void filling composite shell nacre cement. Therefore, to achieve this, first a method was developed to get shell nacre powder from the shells of *Pinctada fucata* and the shell nacre powder was characterized by Fourier transform infrared spectroscopy (FTIR), thermogravimetry (TGA), Raman spectroscopy, X-ray diffractogram (XRD), inductively coupled optical emission spectroscopy (ICP-OES) to confirm the chemical composition. This was followed by the synthesis and characterization of shell nacre containing ladder structured siloxane methacrylate (SN LSM). Further, an *in situ* curing two paste composite shell nacre cement (SNC) was formulated using the synthesized SNLSM and shell nacre powder (24, 48 and 72%) with other additives. Radiopacity, linear polymerization shrinkage and mechanical properties of the cement compositions were investigated and SNC 72 was selected for further studies. The Exotherm generation was studied by isothermal DSC. Finally, cytotoxicity of the SNC was evaluated based on ISO 10993-5[46] with L929 cells.

2. Materials and Methods

2.1. Collection of shells and removal of outer prismatic layer

Pinctada fucata shells which were discarded after the fishing activities were collected from the Kayalpattinum coast of the Gulf of Mannar. The shells were washed in running water and the external impurities like tunicates and deposited dirt were removed mechanically. Followed by the intensive detergent wash, shells were dried at 37 °C. Dried shells were soaked in 15-20% acetic acid with 5%NaCl. After 1 hr of soaking, the external prismatic layer was scrubbed out. Shells were sonicated in distilled water to remove the acid impurities and then dried nacreous shells were observed in scanning electron microscopy (SEM)(FEI Quanta 200, Netherlands).

 doi:10.20944/preprints202305.0422.v1

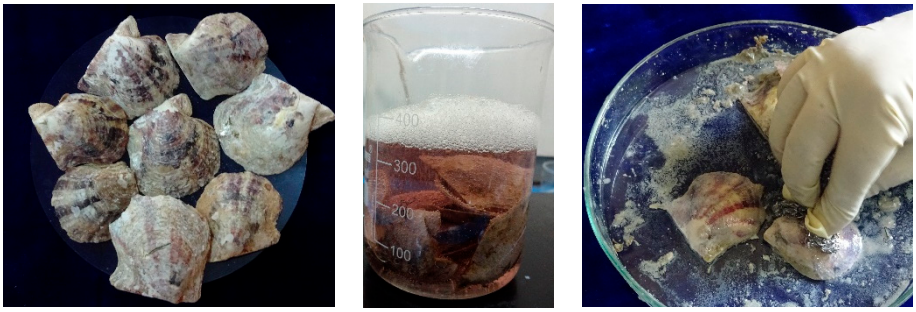

(**a**) (**b**) (**c**)

Figure 1. Processing of pearl oyster shells: (**a**)Shells of *Pinctada fucata*; (**b**) Soaking of shells in acetic acid and NaCl solution and **(c)**scrubbing the outer prismatic layer.

2.1.1. Processing method for shell nacre powder

Nacreous shells were broken into small pieces and powdered using a planetary ball mill (Retsch,Germany) and sieved using a vibrational sieve (Retsch, Germany). Shell nacre powder collected after a 20 μ sieve was purified, characterized, and used for the synthesis of SNLSM resin and as filler for shell nacre cement formulation.

2.1.2. Characterization of shell nacre powder

The particle size and morphology of shell nacre powder was studied by scanning electron microscopy. Shell nacre powder was mixed with potassium bromide (KBr) in the ratio 1:400 and the FTIR spectrum was recorded from 400 -4000 cm^{-1}at a resolution of $4cm^{-1}$(FTIR Carry 600, Agilent technologies). Raman spectrum of shell nacre powder was recorded using confocal Raman microscopy (alpha 300RA, Witec, Germany) with a 532 nm laser. XRD (Bruker, D8 Advance, Germany) was measured in the 2θ range 10°-70°C with CuKά radiation in the incremental step of 5° and peaks were identified using the JCPDS (Joint committee on powder Diffraction standards) database. Thermogravimetry analysis of shell nacre powder was carried out using SDT-2960, TA Instruments and heated from room temperature to 1000°C (heating rate-10°C/min) in a nitrogen atmosphere. Trace elements like Cu, Fe, Mg, Mn, Zn, Cd, Pb,Hg, and Se were estimated using Optical Emission Spectroscopy with Inductively Coupled Plasma (OES-ICP) (Perkin Elmer, US).

2.2. Synthesis of SNLSM 1 and SNLSM 2

The first step in the synthesis was hydrolysis of the precursor 3-trimethoxysilyl propyl methacrylate (Sigma Aldrich) with deionized water in a ratio of 1:3. After 30 mins of hydrolysis, 6N NaOH, shell nacre powder (1%) and diethyl ether were added and the reaction was continued for 8 h to synthesize SNLSM 1 resin. The same procedure was followed for SNLSM 2 resin with 2% shell nacre powder. Later the reaction mix was washed and separated with distilled water and diethyl ether to remove the alkali. Then, the ether phase containing the resin was collected, evaporated, and dried at 37°C till the complete removal of water. The refractive index of the resin was observed using Abbey refractometer (ATAGO 3T, Japan).

2.3. Characterization of SNLSM resins

FTIR of the synthesized resins were measured using the FTIR Carry 600 (Agilent Technologies) spectrum from 400-4000 cm^{-1} at a resolution of 4 cm^{-1}. A thick layer of resin was applied on a glass slide and the Raman spectrum was recorded using confocal Raman microscopy (alpha 300RA, Witec, Germany) with a 532 nm laser. Thermal stability of the resins (SN-LSM1, SN-LSM 2) were evaluated by heating from room temperature to 1000°C at the heating rate was 10°C/min, in a nitrogen atmosphere. The glass transition temperature (Tg) and melting temperature of the resins were measured using differential scanning calorimetry(DSC) (Universal V4.5A, TA Instruments Inc, USA)

Preprints (www.preprints.org) | NOT PEER-REVIEWED | Posted: 6 May 2023 doi:10.20944/preprints202305.0422.v1

under -90°C to 300°C at a ramp rate of 10°C/min, in a nitrogen atmosphere. All graphs were drawn using Origin Pro (version 8.5)

2.4. Formulation of shell nacre cements

Shell nacre cement was formulated with the shell nacre powder and the synthesized SNLSM 2 as a two-paste system A and B. Paste A included SN-LSM 2 (12%), triethylene glycol dimethacrylate (TEGDMA) (12%) (Sigma Aldrich), dimethyl amino phenyl ethanol (DMAPEA) (0.4%) (Sigma Aldrich, US), fumed silica (fs) (3%), traces of 4-methoxy phenol (4-MP) (Sigma Aldrich, US), and shell nacre powder (24/48 / 72%). Paste B included SN-LSM 2 (12%), TEGDMA (12%), benzoyl peroxide (BPO) (0.7%) (Merck, Germany), traces of butylated hydroxytoluene (BHT) (Merck, Germany) and 4-MP, fs (3%), and shell nacre powder (24/48 / 72%). All the percentages mentioned were weight percentage and indicated as (wt.%).

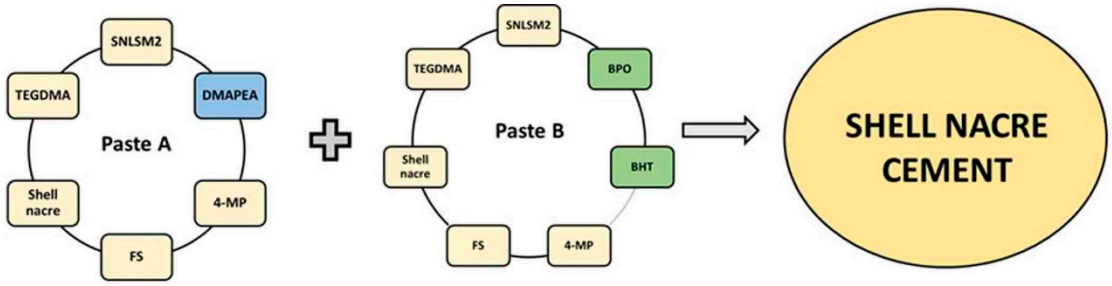

Figure 2. Representation of the formulation of paste A and paste B which were mixed together to prepare the shell nacre cement.

2.4.1. Preparation of Paste A and Paste B (SNC 24/48/72)

First step in the preparation of Paste A was to thin SNLSM 2 with TEGDMA to form the resin matrix. DMAPEA was added next, followed by 4-MP, which were allowed to dissolve completely in the resin matrix. Subsequently, FS was added and mixed well. Finally shell nacre powder was added slowly and mixed thoroughly to form the paste A. Similarly, Paste B was prepared in the same way. BPO, BHT and 4-MP were added to the resin matrix and completely dissolved. Afterward FS was added, and lastly, shell nacre powder was added to form the paste B. Likewise, Paste A and Paste B were individually prepared for all the cements SNC 24, SNC 48 and SNC 72 by varying the amount of shell nacre powder to 24, 48 and 72 wt%.

2.4.2. Preparation of shell nacre cement samples

An equal amount of paste A (SNC 24/48/72) and paste B (SNC 24/48/72) was mixed for 30 sec by hand spatulation. After mixing, the cement was allowed to polymerize and the time before it started to get set was recorded as the working time. The time required for the complete setting of the cement (which was understood by the non-sticky nature of the cement) was noted as setting time. and the cured/set samples of required dimensions were prepared according to the need of experiments.

 doi:10.20944/preprints202305.0422.v1

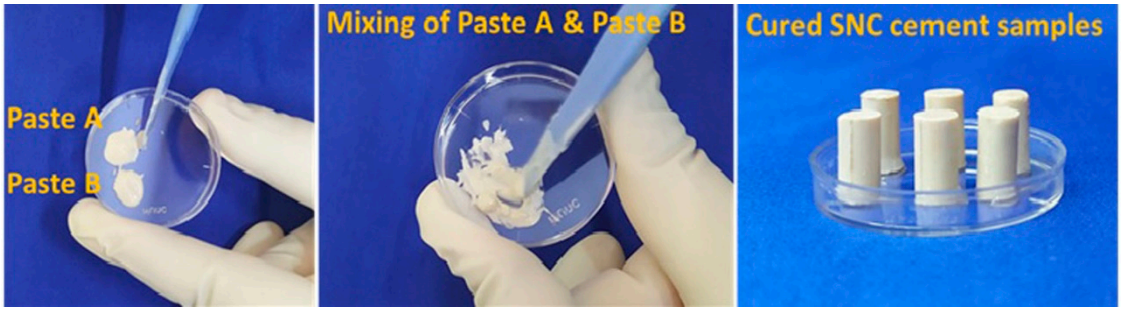

Figure 3. Preparation of shell nacre cement samples; Equal amount of paste A and paste B were mixed together and filled in the mold to get the cured samples of specific dimensions. Here the cured compressive strength samples were shown. .

2.5. Characterization of shell nacre cement

2.5.1. Evaluation of radiopacity

Radiopacity of the cement was studied based on the ASTM standard F640 2012 [47]. Scout images of SNC samples (6mm diameter and 3mm height) and the reference material aluminium step wedge (aluminium alloy EN 1050 containing 99.5% of Al) was acquired using microcomputed tomography (μCT Scanco 40, Switzerland). Using image J, the grayscale intensity of the samples was analysed (n=6). A standard curve was plotted with thickness of Al wedge (0.5, 1, 1.5, 2, 2.5 and 3 mm) against mean grayscale intensity of the Al wedge. Radiopacity of the cement samples equivalent to the thickness of the Al wedge (mm)was determined from the standard curve.

2.5.2. Evaluation of linear polymerization shrinkage (LPS)

Shell nacre cement was packed in a 6mm diameter and 3mm height stainless steel mold and allowed to cure. The sample was then released from the mold and the internal diameter of the mold was calculated accurately using a digital caliper with an accuracy of 0.01 mm (Mitutoyo, Japan). The diameter of the cured sample was measured at six points in all directions and the mean value was calculated. The measurement was repeated for six samples and the percentage linear polymerization shrinkage was calculated [37].

2.5.3. Evaluation of mechanical properties

Compressive strength samples were prepared using the brass mold of 3 mm diameter and 6 mm depth. The mold was placed on a strip of the transparent sheet on a metal plate and the shell nacre cement pastes A and B were mixed and packed into the mold. The second strip of the transparent sheet was placed on the top followed by a second metal plate. The mold and strip of film between the metal plates were pressed to displace excess material and allowed to cure for 30 mins. Similarly, flexural strength test specimens were prepared using the mold of 25 mm length, 2 mm depth, and 2mm thickness. The cured samples were removed from the mold and incubated in distilled water at 37±1^{0}C for 23±1 h and 22±2^{0}C for 1 h before testing. Using the corresponding jigs, compressive strength and flexural strength were determined using a universal testing machine (Instron, Model 1011, UK) with a crosshead speed of 5 mm/min and 1 mm/min respectively.

2.5.4. Investigation of exotherm generated

Exotherm generation of the curing SNC 72 cement was studied by isothermal DSC (Universal V4.5A, TA Instruments Inc, USA) at 24°C and 37°C for 30 min and the enthalpy change (δH) was recorded.

Preprints (www.preprints.org) | NOT PEER-REVIEWED | Posted: 6 May 2023 doi:10.20944/preprints202305.0422.v1

2.5.5. Cytotoxicity evaluation

Cytotoxicity test of the sterile SNC 72 cement sample was performed based on ISO 10993-5 [46]. The positive control used was stabilised polyvinylchloride (PVC) disc and the negative control was ultra-high molecular weight poly ethylene (UHMWPE). All the samples were sterile and with flat surface. L929 mouse fibroblast cells (ATCC) were cultured in Dulbecco's minimal essential media (DMEM; Gibco, USA) supplemented with 10%fetal Bovine serum (FBS, Gibco, USA) and 1% penicillin streptomycin (Gibco, USA). Cells were seeded in a 24 well plate at a density of $3x10^4$ cells/well and incubated at 37°C with 5% CO_2 and allowed to grow till sub confluency. Three replicates of SNC 72 and the controls were placed on the monolayer of L929 cells. After 24 h contact with material, cell monolayer was observed under phase contrast microscope for the response around the materials. Qualitative evaluation based on changes in cell morphology, zone of lysis, vacuolization, detachment, and membrane disintegration was graded on a scale of 0 (none),1(slight), 2(mild), 3 (moderate)and 4(severe).

2.6. Statistical analysis

All statistical analysis were performed using GraphPad Prism (version 9.5.1). An ordinary one-way ANOVA, along with Tukey's multiple comparison test, was performed to compare the linear polymerization shrinkage, compressive and flexural strength of SNC 24, SNC 48 and SNC 72. Differences were considered statistically significant only if $P \leq 0.05$ and the symbol indicated were ns-P>0.05, * - $P \leq 0.05$, ** - P<0.01, ***- P<0.001, ****- P<0.0001. The data are presented as the mean and the standard deviation of the mean.

3. Results

3.1. Shell nacre powder comprised both organic and inorganic constituents

Pinctada fucata shells were soaked in solution of acetic acid and sodium chloride after being thoroughly cleaned. The outer prismatic layer was removed during this process. SEM observation of lustrous nacreous shells (Figure 4 a) exhibited the characteristic brick and mortar structure of shell nacre (Figure 4 b). The lustrous nacreous shells were ball milled and sieved to get the shell nacre powder (Figure 4 c). SEM analysis of the shell powder (Figure 4 d) revealed an irregular morphology with different sizes of approximately 0.2-0.4 μm (Image J analysis).

(a) (b) (c) (d)

Figure 4. Processing of shells.; **(a)** Nacreous shells after prismatic layer removal; **(b)** SEM observation of nacreous shells; **(c)** Macroscopic appearance of shell nacre powder **(d)** SEM observation of shell nacre powder.

FTIR analysis of shell nacre powder is shown in Figure 5 a. The presence of peaks for the internal vibration modes of CO_3^{2-} ions of calcium at 714 cm^{-1},862 cm^{-1}, 1083 cm^{-1} and 1480 cm^{-1} and a splitting peak at 714 cm^{-1} confirmed the aragonite form. The strongest peak of the spectrum was at 1480 cm^{-1}which was due to the overlap of peaks of organic matrix and carbonate ions. The broad peak at 3463 cm^{-1} was the stretching modes of OH/NH of organic matrix, whereas the peak of CH stretching modes were at 2920 cm^{-1}. The peaks of OH of HCO3- groups in the crystal lattice or at the mineral/organic interface groups of carboxylic groups were observed at 2522 cm^{-1} and stretching of carbonyl groups

Preprints (www.preprints.org) | NOT PEER-REVIEWED | Posted: 6 May 2023 doi:10.20944/preprints202305.0422.v1

of acidic proteins at 1785 cm^{-1}. Peaks at 1656 and 1522 cm^{-1} were attributed to the amide I / amide II bonds of proteins of organic matrix.

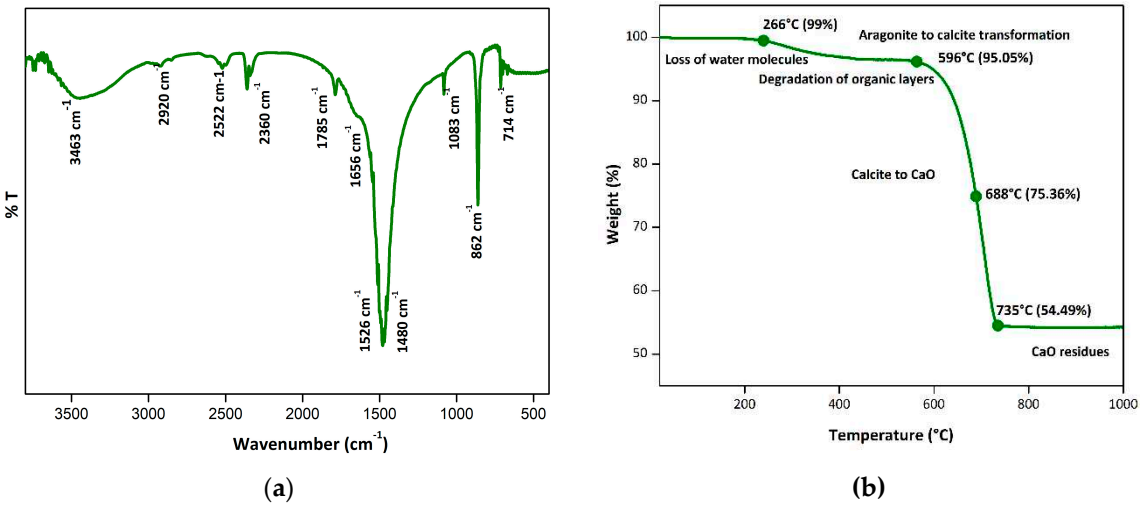

(a) (b)

Figure 5. Characterization of shell nacre powder; **(a)** FTIR spectrum from 400-3750 cm^{-1} and **(b)** Thermogram from RT -1000°C confirming the presence of both organic and inorganic constituents.

The thermogram of shell nacre powder is shown in (Figure 5 b). The initial loss of water content was observed at 266°C, followed by the degradation of organic content at 596°C and the transformation of the aragonite to calcite. The gradual major loss (40%) occurred between 596°C to 735°C during the conversion of calcite to calcium oxide with the release of CO_2 and left with final residue of calcium oxide (56%) at 1000°C.

Micro-Raman spectrum (Figure 6 a) exhibited the characteristic carbonate stretching vibrations of aragonite at 1084 $cm^{-1}$and lattice vibrations modes of aragonite at 155cm^{-1}, 208 $cm^{-1}$and 706 cm^{-1}. X ray diffraction pattern (Figure 6 b) of shell nacre powder matched with the aragonite crystals of JCPDS 01-071-2392 and had characteristic sharp diffraction lines of well crystallized aragonite of single mineral phase. Trace element analysis (Table 1) showed the presence of copper below the detection limit, manganese and zinc were less than a ppm (0.772 & 0.48), iron was 5.8 ppm and the magnesium crossed 102 ppm. Among the deleterious heavy metals, cadmium and selenium were below the detection limit, mercury and lead reached 1.4 ppm and 0.772 ppm.

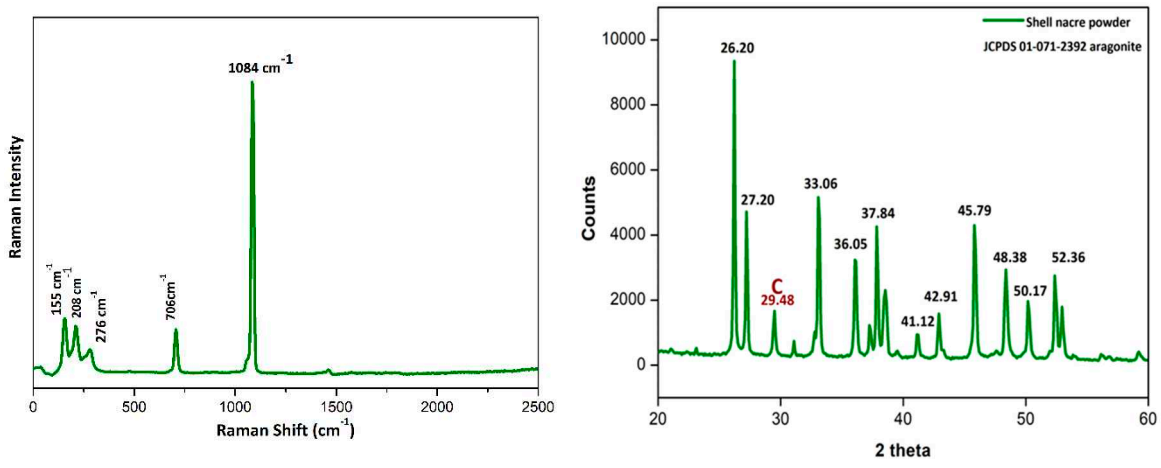

(a) (b)

Figure 6. Characterization of shell nacre powder; **(a)** Micro Raman spectrum and **(b)** X-ray diffraction pattern confirming the aragonite nature of shell nacre powder.

Preprints (www.preprints.org) | NOT PEER-REVIEWED | Posted: 6 May 2023 doi:10.20944/preprints202305.0422.v1

Table 1. ICP OES analysis of shell nacre powder.

Elements analyzed	Total amount (PPM)
Cu	BDL[1]
Fe	5.889
Mg	102.87
Mn	0.772
Zn	0.4827
Cd	BDL[1]
Pb	0.772
Hg	1.4
Se	BDL[1]

[1] BDL Below the lower detection limit for Cu - 0.0097 PPM, Cd - 0.0027 PPM Se - 0.0750 PPM.

3.2. Characterization of SN-LSM 1 and SN LSM 2

FTIR analysis (Figure 7 a) of the resins showed that the broad silanol (Si-OH) peak at 3400-3500 cm^{-1} demonstrated the hydrolysis of the precursor. Bimodal peaks at 1101 cm^{-1} and 1033 cm^{-1} confirmed the polycondensation and formation of ladder structured inorganic siloxane backbone. A shift in the peak from 980 cm^{-1} to 987 cm^{-1} in both the prepolymers confirmed the presence of Si-O-Ca in the network. Further the presence of Ca-O (Figure 7 b) in the siloxane network of SN-LSM was evidenced by a band at 862 cm^{-1}. All the prepolymers retained the characteristic acrylate groups C=C at 1637 cm^{-1} and C=O at 1716 cm^{-1}.

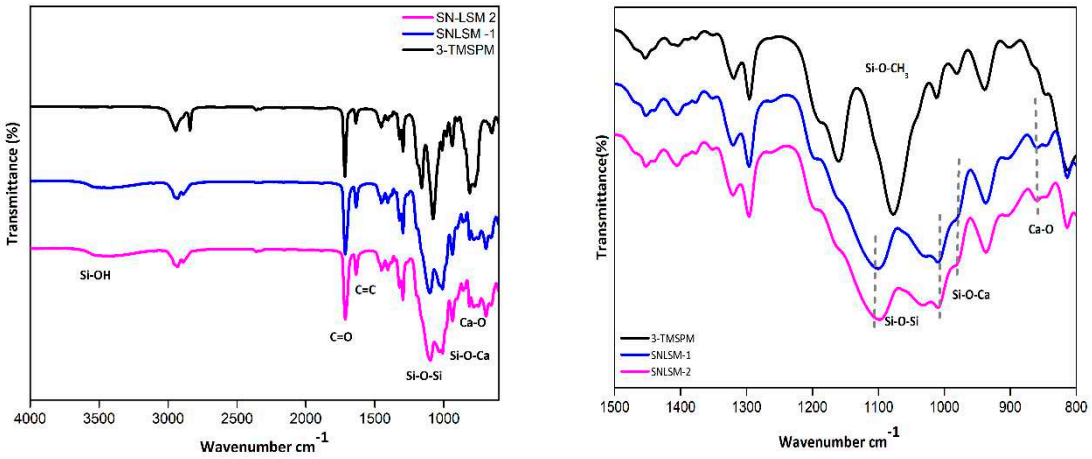

Figure 7. FTIR analysis of SNLSM resin; **(a)** FTIR spectrum from 500-4000 cm^{-1} and **(b)** specific region 800-1500 cm^{-1} showing the ladder structured siloxane methacrylate with integration of shell nacre.

During micro-Raman analysis (Figure 8 a) peaks at 598 cm^{-1} and 1058 cm^{-1}demonstrated the four-membrane structured siloxane ring structure. Further the siloxane network formation was understood by a peak around 829 cm^{-1}. Shift in peaks at 598 cm^{-1},846 cm^{-1}, 900 cm^{-1}, 975 cm^{-1} and 1008 cm^{-1} in both SN LSM1 and SN LSM 2 confirmed the presence of Si-O-Ca in the SNLSM resin.

Preprints (www.preprints.org) | NOT PEER-REVIEWED | Posted: 6 May 2023 doi:10.20944/preprints202305.0422.v1

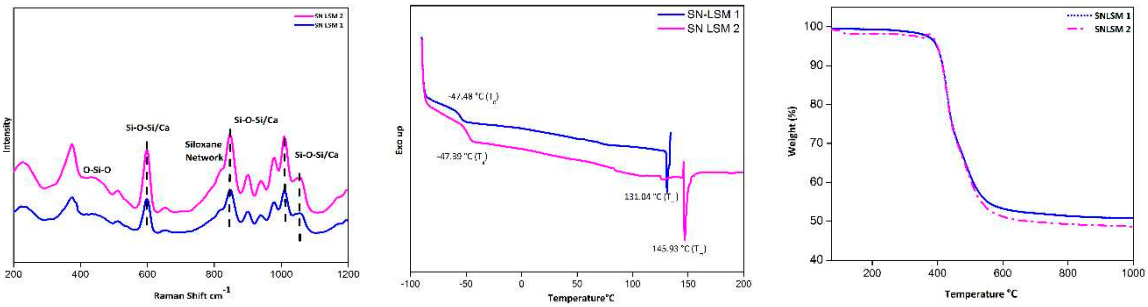

(a) (b) (c)

Figure 8. Characterization of SNLSM; a) Micro Raman spectrum showing the formation of four membered siloxane units; b) Differential scanning calorimetry and c) thermogravimetric analysis of SNLSM 1 and SNLSM 2 confirming the intense siloxane backbone with shell nacre integration.

During DSC investigation (Figure 8 b), low Tg at around -47°C and higher melting peak at 131°C (SNLSM1) and 146°C (SNLSM2) was recorded. Figure 8 c shows the thermogravimetry analysis of the resins at 25°C to 1000°C. The initial degradation started at around 400°C in both SNLSM1 and SNLSM2. SNLSM2 exhibited T_{50} (temperature at which 50% degradation occurred) at 672°C whereas no T_{50} was noted for SNLSM1.

3.3. Radiopaque cement with low linear polymerization shrinkage and better mechanical properties

SNLSM2 showed the presence of shell nacre integrated ladder structured siloxane backbone in all the above characterizations. So SNLSM2 resin was chosen for cement formulations. SNLSM2 (12%) was diluted with equivalent amount of triethylene glycol dimethacrylate (12%) and formulated as a two paste with initiator, activator, stabilizers, fumed silica, and shell nacre powder. Different cement compositions were prepared with increasing quantity of shell nacre powder SNC 24, SNC 48 and SNC 72%. The working time of SNC was 3 min with setting time of 4-10 min .

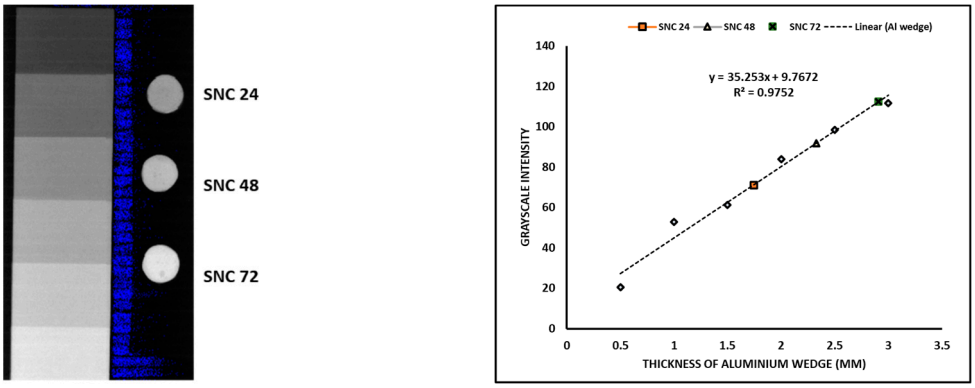

(a) (b)

Figure 9. Radiopacity evaluation; (a)Scout images of shell nacre cement SNC 24, 48 and 72 with Aluminum wedge obtained using micro computed tomography (b) A standard curve was plotted with the thickness of each step of the Al wedge against mean grayscale intensity of the Al step wedge. Radiopacity of the SNC samples equivalent to the thickness of the Al wedge was determined from the standard curve.

SNC 72 exhibited higher radiopacity equivalent to 2.9mm thickness of aluminium wedge. LPS (%) measurements (Figure 10 a) of SNC 72 was 0.4% and significantly lower than other cement compositions ($P<0.0001$). SNC 72 exhibited average compressive and flexural strength of ~110 MPa (Figure 10 b) and of ~35 MPa (Figure 10 c) respectively which is significantly higher than the other cement compositions.

Preprints (www.preprints.org) | NOT PEER-REVIEWED | Posted: 6 May 2023 doi:10.20944/preprints202305.0422.v1

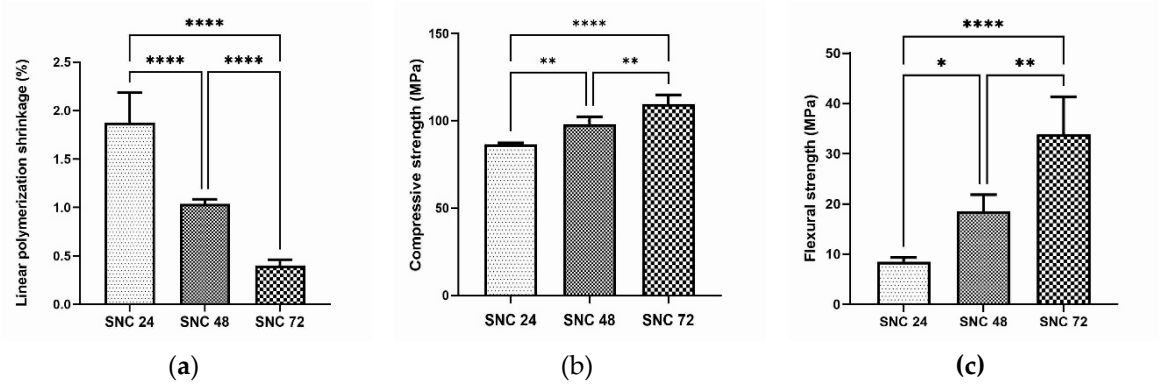

Figure 10. Characterization of shell nacre cement (SNC): a) Evaluation of linear polymerization shrinkage (n=6); b) Compressive strength (n=4); and c) Flexural strength analysis (n=4). Ordinary one-way ANOVA. Tukey's multiple comparisons test. * P< 0.05, ** P<0.01, **** P<0.0001. Data are shown with mean and standard deviation of the mean.

3.4. Minimal exotherm generation and lack of cytotoxicity

The best composition SNC 72 was selected based on the higher compressive strength, flexural strength, radiopacity and lower linear polymerization shrinkage (%) values and continued for further studies. During the curing time of 4-12 mins, composite shell nacre cement SNC 72 generated exotherm (δH) of 0.5781J/g at 24°C (Figure 11 a) and 2.27J/g at 37°C (Figure 11 b).

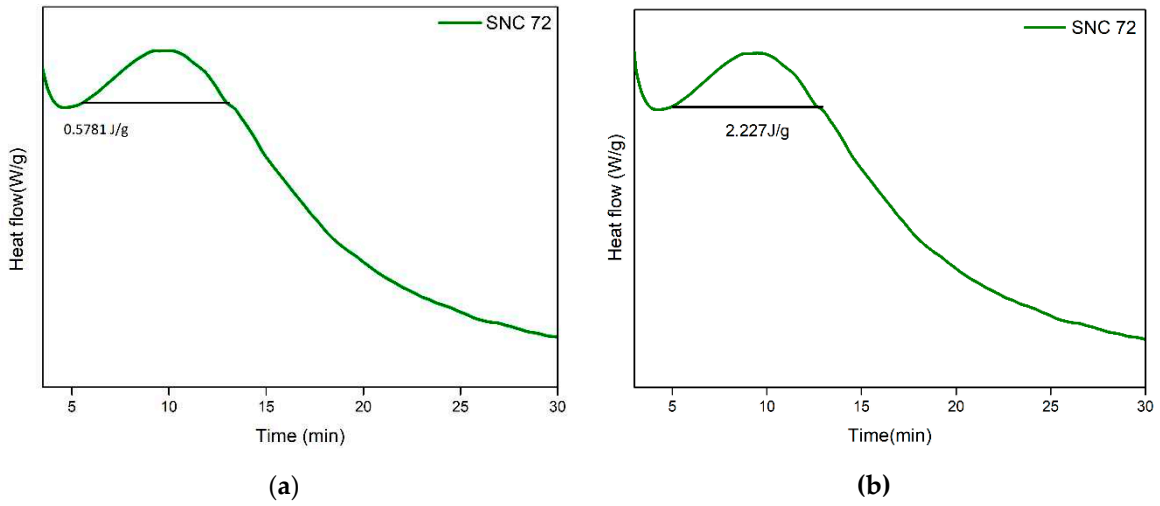

Figure 11. Thermal study of SNC 72: **(a)** Isothermal DSC at 24°C and (**b**) 37°C showing the exotherm generated during the curing of SNC 72.

The cytotoxicity evaluation of SNC 72 was conducted in accordance with ISO 10993-5 using mouse fibroblast cell line L929. After 24h contact with the positive control PVC, L929 cells showed severe cytotoxicity as expected (Figure 12 c) with a grading of 4. During contact with the cured sterile SNC cement sample, L929 cells maintained the spindle morphology and no cytotoxicity features were observed as shown in Figure 12 a. The negative control also showed similar observations (Figure 12 b) and both samples were zero graded. This confirmed the non-cytotoxic nature of the cured shell nacre cement samples.

Preprints (www.preprints.org) | NOT PEER-REVIEWED | Posted: 6 May 2023 doi:10.20944/preprints202305.0422.v1

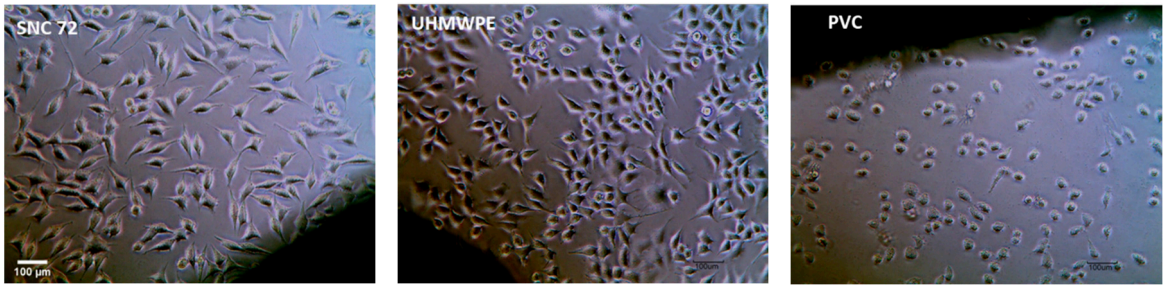

(**a**) (**b**) (c)

Figure 12. Cytotoxicity studies: Direct contact of SNC with L929 cells for 24 h based on ISO 10993-5(a) Shell nacre cement (SNC); (b) Negative control- ultra high molecular weight polyethylene (UHMWPE); (c) Positive control- Poly vinyl chloride disc. Magnification 20 X. Scale bar 100 µm.

4. Discussion

Shell nacre is a superior composite material. So far, only the organic matrix of shell nacre as well as shell nacre pieces or powder, have been studied to demonstrate the osteogenic potential. Although, it is commercially available as a bone substitute in powder form /pieces/osteosynthesis devices [48], there is a void in research where the usage of shell nacre from *Pinctada fucata* is exploited for bone defect management. Another major hurdle is that there is no clear demonstrated processing method to get shell nacre powder with both organic and inorganic parts. This study introduces two novel aspects. Firstly, the shell nacre powder used in the study was comprised of both organic and inorganic constituent and specifically processed from the shells of *Pinctada fucata*. Secondly, shell nacre containing ladder structured siloxane methacrylate resin was used to prepare the *in situ* curing composite cement. This unique composition has not been reported in previous studies, which utilized oyster powder (unnamed) [49], nacre powder (unspecified)[50], clam shell powder [51] or whole abalone shell powder [52] for composite cement preparation. Therefore, to our knowledge, this is the first bone void filling cement of its kind.

The first and foremost task of the present work was to process the shells of *Pinctada fucata* and remove the outer prismatic layer without disturbing the organic layer. For this, different methods like mechanical separation, acid hydrolysis with 5%HCl and hydrogen peroxide, alkali hydrolysis with NaOH have been reported and the amount of organic content was depended on the processing method [53]. Since the objective of the present study was to get shell nacre powder with both inorganic and organic matrix together, a mild acetic acid along with NaCl was attempted. During the process, the shells were soaked in acetic acid and NaCl solution, which enabled the faster removal of calcite with brisk effervescence. Further manual scrubbing completely removed the outer prismatic layer. Subsequently, the lustrous nacreous shells were washed, dried and SEM observation revealed that the aragonite crystals were glued together with the organic matrix, as seen by Sun and Bhushan [54]. The obtained shell nacre powder was heterogenous and irregular with a size of less than 0.5 µm, whereas in other studies shell nacre powder of larger sizes, such as 42.5 µm[55] and 50-100 µm [56] were obtained.

During FTIR study of shell nacre powder, presence of organic peaks of amide I, amide II, OH of water and bicarbonate and inorganic peaks of aragonite confirmed the presence of both organic and inorganic constituents. In the TGA analysis degradation of organic molecules occurred at high temperature 596°C as it is complexed with aragonite. Once the organic content was lost, aragonite crystal got transformed to calcite and gradually the entire calcite got degraded, which was finally left with 56% calcium oxide residues from 735°C. Thus, it was estimated that shell nacre powder comprised of 5% organic and 95% inorganic content which was determined from the thermogravimetry changes. The similar FTIR and TGA results were reported by Balmain *et al.*, and Zouari *et al.*, during the investigation of organic content of the shell nacre of *Pinctada maxima* shells [57] and *Pinctada radiata* shells[58]. Both the Raman and XRD study of shell nacre powder proved the aragonite form of the calcium carbonate as reported. During the analysis, a calcite peak at 276 cm^{-1}

 doi:10.20944/preprints202305.0422.v1

and a diffraction line at 29.4° was of calcite which may be due to the heat generated during the milling of shell nacre powder or may be traces of external prismatic layer or due to presence of calcite in shell nacre itself [57–59]. Further the trace element analysis of SNP was concluded based on ASTM F2103-18 [60] and ASTM F1609 -08[61]. According to the standards, the limit of mercury and lead should be below 5 and 30 ppm and the total content of harmful heavy metal content should be less than 50 ppm. In the present study, shell nacre powder contained mercury and lead which were below the permissive limit and other cadmium, selenium, copper was below the detectable limit. The total deleterious heavy metal content was below 50 ppm and hence shell nacre powder was eligible for biomedical applications. Thus, the acetic acid-based method removed the prismatic layer and yielded shell nacre powder with both organic and inorganic content.

The next objective was synthesis and characterization of the shell nacre containing siloxane methacrylate resin SNLSM. The synthesized resins SNLSM 1 and SNLSM 2 showed no change in refractive index ~1.47 after the addition 1 and 2% shell nacre powder. During the synthesis, the alkoxy silane was hydrolyzed, NaOH favoured the condensation of the silanol moieties and the ladder structured inorganic siloxane network with methacrylate side chain was synthesized. FTIR analysis of the resins proved that the siloxane backbone was ladder structured with intact methacrylate moieties and these results were consistent with the previous studies [42,43,45]. Raman analysis of the resins showed that the siloxane unit was four membered, in agreement with previous findings [62]. The integration of shell nacre was confirmed by both FTIR and Raman analysis, as evidenced by the shift in siloxane peaks and these findings were consistent with the previous research [36]. Highly flexible and partial crystalline siloxane chains were understood by the record of low glass temperature and melting peak[63]. Herein, a low T_g was recorded in both the resins proving the flexibility of the siloxane chains. However, instead of a low melting peak, high melting peak was recorded which may be due to the methacrylate side chains. Further, it was reported that the ladder structured siloxane methacrylate (LSM) were highly thermostable and the LSM resisted the temperature up to 1000°C and left with residue of ~52% [45]. In the present study, SNLSM 1 was left with ~51% residue and no T_{50} was recorded whereas the SNLSM 2 had ~49% residue with T_{50} at 672°C. The record of T_{50} in the case of SNLSM 2 indicated the modification of siloxane network by shell nacre. As SNLSM 2 evidenced the presence of shell nacre in all the above characterization studies, it was further taken for the cement formulation.

Shell nacre cement was as formulated and during the mixing of both paste A and paste B, BPO along with DMAPEA promoted the polymerization of the organic network by breaking the C=C bond of the methacrylate moieties of the resin and TEGDMA and the chain growth was continued. The amount of BPO, DMAPEA and BHT was optimized and the working time of the cement was 3 mins with a setting time of 4- 10mins. Different cements were prepared by varying the amount of shell nacre powder (24, 48 and 72wt%) and the effect on the physico-chemical properties like radiopacity, LPS (%), mechanical properties of the cement was studied.

Radiopacity is essential for the successful clinical monitoring of the material. Barium sulphate and zirconium dioxide is used as radiopacifier in the clinically available PMMA cement. However, the toxicity and effect on mechanical properties demanded alternatives and many other like triphenyl bismuth, tantalum powder, bismuth salicylate, iodine containing co-polymer as powder, as liquid, bromine containing co-polymer [64], gold [65] were investigated as radiopacifier. The radiopacity values of SNC 24, SNC 48 and SNC 72 were 1.74, 2.3, 2.9 mm equivalent to the thickness of Aluminium wedge. Radiopacity was enhanced with increasing concentration of shell nacre and the inherent radiopacity of shell nacre bestowed the cement compositions with radiopacity.

Shrinkage of cement after polymerization is a major concern and the linear polymerization shrinkage of commercially available bone cements were in the range of 5-10% [66]. The exotherm generated by the PMMA cement was 52kJ/mole of PMMA, which was very high and it was the another major drawback of the cement [10].The stability, lack of cytotoxicity and mechanical support determine the healing of any bone defect. So, a bone void filling cement with synergistic properties like mechanical property, non-cytotoxicity, minimal shrinkage and exotherm is necessary. This synergism is achieved by either altering the resin matrix or the filler part.

 doi:10.20944/preprints202305.0422.v1

Both strategies were tried in SNC cement by modifying the organic resin matrix with ormocer SN LSM and introducing shell nacre (24%, 48% and 72 %) in the filler part. Linear polymerization shrinkage percentage of the compositions (24, 48 and 72% shell nacre) was 1.8, 1.03 and 0.4% indicating the reduction in the shrinkage with increasing filler amount. Anyhow, the shrinkage of the minimal shell nacre containing cement was 1.8% which reflected the multi-functionality of SNLSM. Thus, the synergistic action of both the SNLSM and shell nacre reduced the linear polymerization shrinkage of the SNC compositions. Being an inorganic organic hybrid filler, shell nacre was incorporated to the cement compositions without any silanation. Both the ormocer SNLSM and shell nacre contributed to the mechanical properties which was understood by the increase in both compressive and flexural strength with increasing shell nacre content.

Previous studies by Shen *et al*., and Du *et al*., reported that the compressive strength of calcium sulfate composites of oyster powder and abalone shell powder was only ~11 MPa [49] and ~5 MPa [52] respectively. Another study with calcium phosphate cement, showed that increasing concentration of nacre reduced the compressive strength [50]. In contrast, the compressive strength of the current SNC 72 composite was ~110 MPa which was 10- 20 times higher than the reported calcium sulfate composites, and the mechanical properties were further enhanced with increasing shell nacre content. Previous studies by Wu *et al*., reported that addition of amphiphilic raspberry particles to the PMMA reduced the compressive strength [67]. Similarly, addition of magnesium oxide also reduced the mechanical properties of the cement[68]. However, in the shell nacre cement compositions, the mechanical properties were improved by the bonding of shell nacre powder with the SNLSM resin. A study by Yang *et al*., found that use of acrylic acid and styrene in PMMA cement lowered the compressive strength than PMMA [69]. But in the present cement, SNLSM imparted good compressive strength even to the cement with low concentration of shell nacre powder (24 wt%).

SNC 72 exhibited better mechanical property, radiopacity and low linear polymerization shrinkage and so selected for further studies like isothermal DSC and cytotoxicity. As curing is affected by temperature, both the room temperature of the surgery room and the human body temperature was considered and isothermal DSC was carried out at both 24°C and 37°C. Although the heating rate and other conditions were similar, variations in enthalpy change δH was found owing to curing of SNC in two different temperatures. The exotherm generated by SNC 72 at 37°C was 2.27J/g which may be due to the fast curing of the cement and the slow curing at 24°C liberated exotherm of only 0.5781J/g. A previous study reported no significant change in maximum polymerization temperature of Palacos cement after modification with 2-hydroxyethyl methacrylate, calcium chloride and sodium carbonate [70]. Similarly, addition of graphene and graphene oxide powders to PMMA showed no changes in exotherm generation [71]. In contrast, combination of shell nacre powder and SNLSM resulted in the reduction of exotherm, which was very minimal when compared to the commercially available cements and experimental cements.

SNC 72 comprised 72wt% of shell nacre, 12wt% of SNLSM 2 and TEGDMA and the complete curing of the cement was favoured by BPO and DMAPEA. L929 cells retained the spindle morphology after 24 h contact with the cured SNC 72 cement and the observations were very similar to that of negative control. This indirectly ensured the complete curing of SNC 72 with no monomer toxicity and so the L929 cells showed no features of toxicity. A previous study found that addition of increasing amount of calcium sulfate (40% by weight) to PMMA cement resulted in the reduction of cell viability [72]. On the other hand, higher addition of shell nacre (72 % by weight) to SNC 72 did not cause any toxicity issues due to its biocompatibility. SNC 72 was radiopaque and non-cytotoxic, with better mechanical properties, low linear polymerization shrinkage and minimal exotherm generation. Therefore, the findings from the study proved that the shell nacre cement will be a potential bone void filling cement for bone defect management.

5. Conclusions

In this work, we successfully developed a processing method to get shell nacre powder, synthesized shell nacre containing ladder structured siloxane methacrylate and formulated a non-

cytotoxic bone void filling cement with good physicochemical properties. Synergistic action of both ormocer SNLSM resin and shell nacre filler contributed to the better mechanical properties, minimal shrinkage and exotherm. Further insights into the osteogenesis, biocompatibility, osseointegration will demonstrate the biological performance of the cement.

6. Patents

Lizymol Philiphose Pampadykandathil, Bridget Jeyatha Wilson, and Venkiteswaran Kalliyanakrishnan. 2018. A process for the synthesis of shell nacre containing bio-resin for dental and orthopedic applications. Indian patent No.400578. Date of Grant: 30/06/2022.

Lizymol Philiphose Pampadykandathil and Bridget Jeyatha Wilson. 2020. Low-cost bioactive bone cement. Indian patent No. 410827. Date of Grant: 02/11/2022.

Author Contributions: Conceptualization WBJ and LPP; methodology WBJ; software WBJ; validation, WBJ; formal analysis WBJ ; investigation, WBJ and LPP ; resources, WBJ; data curation,WBJ; writing—original draft preparation; writing—review and editing, WBJ and LPP; visualization, WBJ and LPP; supervision, LPP; project administration, LPP; funding acquisition, LPP. All authors have read and agreed to the published version of the manuscript.

Funding: LPP thank Kerala State Council for Science Technology and Environment KSCSTE (009/ SRSHS/2014/CSTE). WBJ thank KSCSTE and Indian Council for Medical Research – ICMR for the fellowship (ICMR 3/1/2/ 2(SRF) Ortho/2018-NCD-I). Authors thank authorities of SCTIMST

Informed Consent Statement: Not applicable

Acknowledgments: Authors thank Dr. Kavitha, Shellfish Fisheries Division, Central Marine Fisheries Research Institute, Tuticorin, India for the species confirmation of the shells.

Conflicts of Interest: The authors declare no conflict of interest. The funders had no role in the design of the study; in the collection, analyses, or interpretation of data; in the writing of the manuscript; or in the decision to publish the results".

References

1. Mancuso, F.; Beltrame, A.; Colombo, E.; Miani, E.; Bassini, F. Management of Metaphyseal Bone Loss in Revision Knee Arthroplasty. *Acta Biomed* **2017**, *88*, 98–111, doi:10.23750/abm.v88i2-S.6520.
2. Hasandoost, L.; Rodriguez, O.; Alhalawani, A.; Zalzal, P.; Schemitsch, E.H.; Waldman, S.D.; Papini, M.; Towler, M.R. The Role of Poly(Methyl Methacrylate) in Management of Bone Loss and Infection in Revision Total Knee Arthroplasty: A Review. *JFB* **2020**, *11*, 25, doi:10.3390/jfb11020025.
3. Blokhuis, T.J. Management of Traumatic Bone Defects: Metaphyseal versus Diaphyseal Defects. *Injury* **2017**, *48*, S91–S93, doi:10.1016/j.injury.2017.04.021.
4. Piccirilli, E.; Cariati, I.; Primavera, M.; Triolo, R.; Gasbarra, E.; Tarantino, U. Augmentation in Fragility Fractures, Bone of Contention: A Systematic Review. *BMC Musculoskelet Disord* **2022**, *23*, 1046, doi:10.1186/s12891-022-06022-0.
5. He, Z.; Zhai, Q.; Hu, M.; Cao, C.; Wang, J.; Yang, H.; Li, B. Bone Cements for Percutaneous Vertebroplasty and Balloon Kyphoplasty: Current Status and Future Developments. *Journal of Orthopaedic Translation* **2015**, *3*, 1–11, doi:10.1016/j.jot.2014.11.002.
6. Reito, A.; Ylitalo, A. Polymethyl Methacrylate Cement Fill as a Definitive Treatment for Massive Bone Defect After Infected Internal Fixation in Bicondylar Tibial Fracture: A Case Report. *JBJS Case Connector* **2020**, *10*, e19.00286, doi:10.2106/JBJS.CC.19.00286.
7. Wu, M.; Yao, S.; Xie, Y.; Yan, F.; Deng, Z.; Lei, J.; Cai, L. A Novel Subchondral Bone-Grafting Procedure for the Treatment of Giant-Cell Tumor around the Knee: A Retrospective Study of 27 Cases. *Medicine (Baltimore)* **2018**, *97*, e13154, doi:10.1097/MD.0000000000013154.
8. Vaishya, R.; Chauhan, M.; Vaish, A. Bone Cement. *Journal of Clinical Orthopaedics and Trauma* **2013**, *4*, 157–163, doi:10.1016/j.jcot.2013.11.005.
9. O'dowd-Booth, C.J.; White, J.; Smitham, P.; Khan, W.; Marsh, D.R. Bone Cement: Perioperative Issues, Orthopaedic Applications and Future Developments. *Journal of Perioperative Practice* **2011**, *21*, 304–308, doi:10.1177/175045891102100902.

10. Soleymani Eil Bakhtiari, S.; Bakhsheshi-Rad, H.R.; Karbasi, S.; Tavakoli, M.; Razzaghi, M.; Ismail, A.F.; RamaKrishna, S.; Berto, F. Polymethyl Methacrylate-Based Bone Cements Containing Carbon Nanotubes and Graphene Oxide: An Overview of Physical, Mechanical, and Biological Properties. *Polymers (Basel)* **2020**, *12*, E1469, doi:10.3390/polym12071469.
11. Kawanabe, K.; Tamura, J.; Yamamuro, T.; Nakamura, T.; Kokubo, T.; Yoshihara, S. A New Bioactive Bone Cement Consisting of BIS-GMA Resin and Bioactive Glass Powder. *Journal of Applied Biomaterials* **1993**, *4*, 135–141, doi:10.1002/jab.770040204.
12. Mousa, W.F.; Kobayashi, M.; Shinzato, S.; Kamimura, M.; Neo, M.; Yoshihara, S.; Nakamura, T. Biological and Mechanical Properties of PMMA-Based Bioactive Bone Cements. *Biomaterials* **2000**, *21*, 2137–2146, doi:10.1016/S0142-9612(00)00097-1.
13. Goto, K.; Tamura, J.; Shinzato, S.; Fujibayashi, S.; Hashimoto, M.; Kawashita, M.; Kokubo, T.; Nakamura, T. Bioactive Bone Cements Containing Nano-Sized Titania Particles for Use as Bone Substitutes. *Biomaterials* **2005**, *26*, 6496–6505, doi:10.1016/j.biomaterials.2005.04.044.
14. Deb, S.; Aiyathurai, L.; Roether, J.A.; Luklinska, Z.B. Development of High-Viscosity, Two-Paste Bioactive Bone Cements. *Biomaterials* **2005**, *26*, 3713–3718, doi:10.1016/j.biomaterials.2004.09.065.
15. Ni, G.X.; Chiu, K.Y.; Lu, W.W.; Wang, Y.; Zhang, Y.G.; Hao, L.B.; Li, Z.Y.; Lam, W.M.; Lu, S.B.; Luk, K.D.K. Strontium-Containing Hydroxyapatite Bioactive Bone Cement in Revision Hip Arthroplasty. *Biomaterials* **2006**, *27*, 4348–4355, doi:10.1016/j.biomaterials.2006.03.048.
16. Liu, Z.; Tang, Y.; Kang, T.; Rao, M.; Li, K.; Wang, Q.; Quan, C.; Zhang, C.; Jiang, Q.; Shen, H. Synergistic Effect of HA and BMP-2 Mimicking Peptide on the Bioactivity of HA/PMMA Bone Cement. *Colloids Surf B Biointerfaces* **2015**, *131*, 39–46, doi:10.1016/j.colsurfb.2015.04.032.
17. Erbe, E.M.; Clineff, T.D.; Gualtieri, G. Comparison of a New Bisphenol-a-Glycidyl Dimethacrylate-Based Cortical Bone Void Filler with Polymethyl Methacrylate. *Eur Spine J* **2001**, *10*, S147–S152, doi:10.1007/s005860100288.
18. Zhang, H.; Cui, Y.; Zhuo, X.; Kim, J.; Li, H.; Li, S.; Yang, H.; Su, K.; Liu, C.; Tian, P.; et al. Biological Fixation of Bioactive Bone Cement in Vertebroplasty: The First Clinical Investigation of Borosilicate Glass (BSG) Reinforced PMMA Bone Cement. *ACS Appl. Mater. Interfaces* **2022**, *14*, 51711–51727, doi:10.1021/acsami.2c15250.
19. Tan, Q.-C.; Jiang, X.-S.; Chen, L.; Huang, J.-F.; Zhou, Q.-X.; Wang, J.; Zhao, Y.; Zhang, B.; Sun, Y.-N.; Wei, M.; et al. Bioactive Graphene Oxide-Functionalized Self-Expandable Hydrophilic and Osteogenic Nanocomposite for Orthopaedic Applications. *Materials Today Bio* **2023**, *18*, 100500, doi:10.1016/j.mtbio.2022.100500.
20. Han, Z.; Wang, B.; Ren, B.; Liu, Y.; Zhang, N.; Wang, Z.; Liu, J.; Mao, K. Characterization and Biomechanical Study of a Novel Magnesium Potassium Phosphate Cement. *Life (Basel)* **2022**, *12*, 997, doi:10.3390/life12070997.
21. Moore, W.R.; Graves, S.E.; Bain, G.I. Synthetic Bone Graft Substitutes. *ANZ Journal of Surgery* **2001**, *71*, 354–361, doi:10.1046/j.1440-1622.2001.02128.x.
22. Nandi, S.K.; Roy, S.; Mukherjee, P.; Kundu, B.; De, D.K.; Basu, D. Orthopaedic Applications of Bone Graft & Graft Substitutes: A Review. *Indian Journal of Medical Research* **2010**, *132*, 15.
23. Wang, W.; Yeung, K.W.K. Bone Grafts and Biomaterials Substitutes for Bone Defect Repair: A Review. *Bioactive Materials* **2017**, *2*, 224–247, doi:10.1016/j.bioactmat.2017.05.007.
24. Marongiu, G.; Verona, M.; Cardoni, G.; Capone, A. Synthetic Bone Substitutes and Mechanical Devices for the Augmentation of Osteoporotic Proximal Humeral Fractures: A Systematic Review of Clinical Studies. *Journal of Functional Biomaterials* **2020**, *11*, 29, doi:10.3390/jfb11020029.
25. Fillingham, Y.; Jacobs, J. Bone Grafts and Their Substitutes. *The Bone & Joint Journal* **2016**, *98-B*, 6–9, doi:10.1302/0301-620X.98B.36350.
26. Gu, X.; Li, Y.; Qi, C.; Cai, K. Biodegradable Magnesium Phosphates in Biomedical Applications. *J. Mater. Chem. B* **2022**, *10*, 2097–2112, doi:10.1039/D1TB02836G.
27. Liu, Z.; He, X.; Chen, S.; Yu, H. Advances in the Use of Calcium Silicate-Based Materials in Bone Tissue Engineering. *Ceramics International* **2023**, doi:10.1016/j.ceramint.2023.03.063.
28. Atlan, G.; Delattre, O.; Berland, S.; LeFaou, A.; Nabias, G.; Cot, D.; Lopez, E. Interface between Bone and Nacre Implants in Sheep. *Biomaterials* **1999**, *20*, 1017–1022, doi:10.1016/S0142-9612(98)90212-5.
29. Camprasse, S.; Camprasse, G.; Pouzol, M.; Lopez, E. Artificial Dental Root Made of Natural Calcium Carbonate (Bioracine). *Clinical Materials* **1990**, *5*, 235–250, doi:10.1016/0267-6605(90)90022-N.

30. Lamghari, M.; Berland, S.; Laurent, A.; Huet, H.; Lopez, E. Bone Reactions to Nacre Injected Percutaneously into the Vertebrae of Sheep. *Biomaterials* **2001**, *22*, 555–562, doi:10.1016/S0142-9612(00)00213-1.
31. Berland, S.; Delattre, O.; Borzeix, S.; Catonné, Y.; Lopez, E. Nacre/Bone Interface Changes in Durable Nacre Endosseous Implants in Sheep. *Biomaterials* **2005**, *26*, 2767–2773, doi:10.1016/j.biomaterials.2004.07.019.
32. Kim, H.; Lee, K.; Ko, C.-Y.; Kim, H.-S.; Shin, H.-I.; Kim, T.; Lee, S.H.; Jeong, D. The Role of Nacreous Factors in Preventing Osteoporotic Bone Loss through Both Osteoblast Activation and Osteoclast Inactivation. *Biomaterials* **2012**, *33*, 7489–7496, doi:10.1016/j.biomaterials.2012.06.098.
33. Lee, K.; Kim, H.; Kim, J.M.; Chung, Y.H.; Lee, T.Y.; Lim, H.-S.; Lim, J.-H.; Kim, T.; Bae, J.S.; Woo, C.-H.; et al. Nacre-Driven Water-Soluble Factors Promote Wound Healing of the Deep Burn Porcine Skin by Recovering Angiogenesis and Fibroblast Function. *Mol Biol Rep* **2012**, *39*, 3211–3218, doi:10.1007/s11033-011-1088-4.
34. Gerhard, E.M.; Wang, W.; Li, C.; Guo, J.; Ozbolat, I.T.; Rahn, K.M.; Armstrong, A.D.; Xia, J.; Qian, G.; Yang, J. Design Strategies and Applications of Nacre-Based Biomaterials. *Acta Biomaterialia* **2017**, *54*, 21–34, doi:10.1016/j.actbio.2017.03.003.
35. Zhang, G.; Brion, A.; Willemin, A.-S.; Piet, M.-H.; Moby, V.; Bianchi, A.; Mainard, D.; Galois, L.; Gillet, P.; Rousseau, M. Nacre, a Natural, Multi-Use, and Timely Biomaterial for Bone Graft Substitution. *Journal of Biomedical Materials Research Part A* **2017**, *105*, 662–671, doi:10.1002/jbm.a.35939.
36. Sol–Gel Based Materials for Biomedical Applications - ScienceDirect Available online: https://www.sciencedirect.com/science/article/pii/S0079642516000025 (accessed on 9 April 2020).
37. Lizymol, P.P. Studies on Shrinkage, Depth of Cure, and Cytotoxic Behavior of Novel Organically Modified Ceramic Based Dental Restorative Resins. *Journal of Applied Polymer Science* **2010**, *116*, 2645–2650, doi:10.1002/app.31762.
38. Lizymol, P.P. Effects of Diluent's Concentration upon the Properties of Organically Modified Ceramics Based Composites for Application in Dentistry. *Journal of Applied Polymer Science* **2004**, *94*, 469–473, doi:10.1002/app.20891.
39. Vibha, C.; Lizymol, P.P. Development of Hydroxyapatite-Reinforced Biocomposites Based on Polymerizable Multifunctional Strontium Containing Inorganic-Organic Hybrid Resins for Biomedical Applications. *Materials Letters* **2017**, *197*, 63–66, doi:10.1016/j.matlet.2017.03.098.
40. Vibha, C.; Lizymol, P.P. Synthesis and Characterization of a Novel Radiopaque Dimethacrylate Zirconium Containing Pre-Polymer for Biomedical Applications. *Materials Letters* **2019**, *237*, 294–297, doi:10.1016/j.matlet.2018.11.098.
41. Wolter, H.; Glaubitt, W.; Rose, K. Multifunctional (Meth)Acrylate Alkoxysilanes a New Type of Reactive Compounds. *MRS Online Proceedings Library* **1992**, *271*, 719–724, doi:10.1557/PROC-271-719.
42. Dirè, S.; Borovin, E.; Ribot, F. Architecture of Silsesquioxanes. In *Handbook of Sol-Gel Science and Technology: Processing, Characterization and Applications*; Klein, L., Aparicio, M., Jitianu, A., Eds.; Springer International Publishing: Cham, 2018; pp. 3119–3151 ISBN 978-3-319-32101-1.
43. Kim, Y.H.; Choi, G.-M.; Bae, J.G.; Kim, Y.H.; Bae, B.-S. High-Performance and Simply-Synthesized Ladder-Like Structured Methacrylate Siloxane Hybrid Material for Flexible Hard Coating. *Polymers* **2018**, *10*, 449, doi:10.3390/polym10040449.
44. Haas, K.-H. Hybrid Inorganic–Organic Polymers Based on Organically Modified Si-Alkoxides. *Advanced Engineering Materials* **2000**, *2*, 571–582, doi:10.1002/1527-2648(200009)2:9<571::AID-ADEM571>3.0.CO;2-M.
45. Bridget Jeyatha, W.; Paul, W.; Mani, S.; Lizymol, P.P. Synthesis and Characterization of Ladder Structured Ormocer Resin of Siloxane Backbone and Methacrylate Side Chain. *Materials Letters* **2022**, *310*, 131192, doi:10.1016/j.matlet.2021.131192.
46. INTERNATIONAL STANDARD ISO 10993-5.Biological Evaluation of Medical Devices —Part 5: Tests for in Vitro Cytotoxicity.
47. Standard Test Methods for Determining Radiopacity for Medical Use Available online: https://www.astm.org/f0640-20.html (accessed on 27 February 2023).
48. Orthopaedics | Bone Repair. *MEGA BIOPHARMA*.
49. Shen, Y.; Yang, S.; Liu, J.; Xu, H.; Shi, Z.; Lin, Z.; Ying, X.; Guo, P.; Lin, T.; Yan, S.; et al. Engineering Scaffolds Integrated with Calcium Sulfate and Oyster Shell for Enhanced Bone Tissue Regeneration. *ACS Appl. Mater. Interfaces* **2014**, *6*, 12177–12188, doi:10.1021/am501448t.

50. Ruan, R.; Zheng, M.; Gao, J.; Landao-Bassonga, E.; Chen, L.; Chen, P.; Wang, T.; Zhao, X. Improved Biological Properties of Calcium Phosphate Cement by Nacre Incorporation: An In Vitro Study. *Journal of Biomaterials and Tissue Engineering* **2018**, *8*, 67–79, doi:10.1166/jbt.2018.1720.
51. Simu, M.-R.; Pall, E.; Radu, T.; Miclaus, M.; Culic, B.; Mesaros, A.-S.; Muntean, A.; Filip, G.A. Development of a Novel Biomaterial with an Important Osteoinductive Capacity for Hard Tissue Engineering. *Tissue and Cell* **2018**, *52*, 101–107, doi:10.1016/j.tice.2018.04.004.
52. Du, M.; Li, Q.; Chen, J.; Liu, K.; Song, C. Design and Characterization of Injectable Abalone Shell/Calcium Sulfate Bone Cement Scaffold for Bone Defect Repair. *Chemical Engineering Journal* **2021**, *420*, 129866, doi:10.1016/j.cej.2021.129866.
53. Pei, J.; Wang, Y.; Zou, X.; Ruan, H.; Tang, C.; Liao, J.; Si, G.; Sun, P. Extraction, Purification, Bioactivities and Application of Matrix Proteins From Pearl Powder and Nacre Powder: A Review. *Frontiers in Bioengineering and Biotechnology* **2021**, *9*.
54. Sun, J.; Bhushan, B. Hierarchical Structure and Mechanical Properties of Nacre: A Review. *RSC Adv.* **2012**, *2*, 7617–7632, doi:10.1039/C2RA20218B.
55. Iandolo, D.; Laroche, N.; Nguyen, D.K.; Normand, M.; Met, C.; Zhang, G.; Vico, L.; Mainard, D.; Rousseau, M. Preclinical Safety Study of Nacre Powder in an Intraosseous Sheep Model. *BMJ Open Science* **2022**, *6*, doi:10.1136/bmjos-2021-100231.
56. Atlan, G.; Balmain, N.; Berland, S.; Vidal, B.; Lopez, É. Reconstruction of Human Maxillary Defects with Nacre Powder: Histological Evidence for Bone Regeneration. *Comptes Rendus de l'Académie des Sciences - Series III - Sciences de la Vie* **1997**, *320*, 253–258, doi:10.1016/S0764-4469(97)86933-8.
57. Balmain, J.; Hannoyer, B.; Lopez, E. Fourier Transform Infrared Spectroscopy (FTIR) and X-Ray Diffraction Analyses of Mineral and Organic Matrix during Heating of Mother of Pearl (Nacre) from the Shell of the Mollusc Pinctada Maxima. *Journal of Biomedical Materials Research* **1999**, *48*, 749–754, doi:10.1002/(SICI)1097-4636(1999)48:5<749::AID-JBM22>3.0.CO;2-P.
58. Bellaaj-Zouari, A.; Chérif, K.; Elloumi-Hannachi, I.; Slimane, N.; Jaafoura, M.H. Characterization of Mineral and Organic Phases in Nacre of the Invasive Pearl Oyster Pinctada Radiata (Leach, 1814).
59. In Vivo Characterization of Bivalve Larval Shells: A Confocal Raman Microscopy Study | Journal of The Royal Society Interface Available online: https://royalsocietypublishing.org/doi/full/10.1098/rsif.2017.0723 (accessed on 28 February 2023).
60. Standard Guide for Characterization and Testing of Chitosan Salts as Starting Materials Intended for Use in Biomedical and Tissue-Engineered Medical Product Applications Available online: https://www.astm.org/f2103-18.html (accessed on 25 February 2023).
61. Standard Specification for Calcium Phosphate Coatings for Implantable Materials Available online: https://www.astm.org/f1609-08r14.html (accessed on 28 February 2023).
62. Baatti, A.; Erchiqui, F.; Bébin, P.; Godard, F.; Bussières, D. A Two-Step Sol-Gel Method to Synthesize a Ladder Polymethylsilsesquioxane Nanoparticles. *Advanced Powder Technology* **2017**, *28*, 1038–1046, doi:10.1016/j.apt.2017.01.009.
63. Mark, J.E. Some Interesting Things about Polysiloxanes. *Acc. Chem. Res.* **2004**, *37*, 946–953, doi:10.1021/ar030279z.
64. Lewis, G. Alternative Acrylic Bone Cement Formulations for Cemented Arthroplasties: Present Status, Key Issues, and Future Prospects. *J Biomed Mater Res B Appl Biomater* **2008**, *84*, 301–319, doi:10.1002/jbm.b.30873.
65. Jacobs, E.; Saralidze, K.; Roth, A.K.; de Jong, J.J.A.; van den Bergh, J.P.W.; Lataster, A.; Brans, B.T.; Knetsch, M.L.W.; Djordjevic, I.; Willems, P.C.; et al. Synthesis and Characterization of a New Vertebroplasty Cement Based on Gold-Containing PMMA Microspheres. *Biomaterials* **2016**, *82*, 60–70, doi:10.1016/j.biomaterials.2015.12.024.
66. Gilbert, J.L.; Hasenwinkel, J.M.; Wixson, R.L.; Lautenschlager, E.P. A Theoretical and Experimental Analysis of Polymerization Shrinkage of Bone Cement: A Potential Major Source of Porosity. *Journal of Biomedical Materials Research* **2000**, *52*, 210–218, doi:10.1002/1097-4636(200010)52:1<210::AID-JBM27>3.0.CO;2-R.
67. Wu, T.; Gao, S.; Cui, Y.; Qiao, Y.; Zhou, F.; Qiu, D. Amphiphilic Bioactive Filler for Acrylic Bone Cement to Enhance Its Cell Adhesion. *Journal of Biomedical Nanotechnology* **2018**, *14*, 795–801, doi:10.1166/jbn.2018.2543.
68. Khandaker, M.; Vaughan, M.B.; Morris, T.L.; White, J.J.; Meng, Z. Effect of Additive Particles on Mechanical, Thermal, and Cell Functioning Properties of Poly(Methyl Methacrylate) Cement. *Int J Nanomedicine* **2014**, *9*, 2699–2712, doi:10.2147/IJN.S61964.

69. Yang, Z.; Chen, L.; Hao, Y.; Zang, Y.; Zhao, X.; Shi, L.; Zhang, Y.; Feng, Y.; Xu, C.; Wang, F.; et al. Synthesis and Characterization of an Injectable and Hydrophilous Expandable Bone Cement Based on Poly(Methyl Methacrylate). *ACS Appl. Mater. Interfaces* **2017**, *9*, 40846–40856, doi:10.1021/acsami.7b12983.
70. Wolf-Brandstetter, C.; Roessler, S.; Storch, S.; Hempel, U.; Gbureck, U.; Nies, B.; Bierbaum, S.; Scharnweber, D. Physicochemical and Cell Biological Characterization of PMMA Bone Cements Modified with Additives to Increase Bioactivity. *Journal of Biomedical Materials Research Part B: Applied Biomaterials* **2013**, *101B*, 599–609, doi:10.1002/jbm.b.32862.
71. Paz, E.; Forriol, F.; Del Real, J.C.; Dunne, N. Graphene Oxide versus Graphene for Optimisation of PMMA Bone Cement for Orthopaedic Applications. *Mater Sci Eng C Mater Biol Appl* **2017**, *77*, 1003–1011, doi:10.1016/j.msec.2017.03.269.
72. Chiang, C.-C.; Hsieh, M.-K.; Wang, C.-Y.; Tuan, W.-H.; Lai, P.-L. Cytotoxicity and Cell Response of Preosteoblast in Calcium Sulfate-Augmented PMMA Bone Cement. *Biomed Mater* **2021**, *16*, doi:10.1088/1748-605X/ac1ab5.